www.elsevier.com/locate/ijadhadh

A finite element study of fatigue crack propagation in single lap bonded joint with process-induced disbond

Yiding Liu, Stuart Lemanski, Xiang Zhang, David Ayre, Hamed Yazdani Nezhad

PII: S0143-7496(18)30235-5
DOI: https://doi.org/10.1016/j.ijadhadh.2018.10.005
Reference: JAAD2276

To appear in: *International Journal of Adhesion and Adhesives*
Accepted date: 30 September 2018

Cite this article as: Yiding Liu, Stuart Lemanski, Xiang Zhang, David Ayre and Hamed Yazdani Nezhad, A finite element study of fatigue crack propagation in single lap bonded joint with process-induced disbond, *International Journal of Adhesion and Adhesives,* https://doi.org/10.1016/j.ijadhadh.2018.10.005

International Journal of Adhesion and Adhesives, Volume 87, December 2018, pp. 164-172
DOI: 10.1016/j.ijadhadh.2018.10.005

A finite element study of fatigue crack propagation in single lap bonded joint with process-induced disbond

Yiding Liu[a], Stuart Lemanski[a], Xiang Zhang[a,*], David Ayre[b] and Hamed Yazdani Nezhad[b]

[a]Institute for future transport and cities, Coventry University, CV1 5FB, United Kingdom

[b]Enhanced Composites and Structures Centre, School of Aerospace, Transport and Manufacturing, Cranfield University, MK43 0AL, United Kingdom

[*] Corresponding author. Email address: xiang.zhang@coventry.ac.uk

Abstract

This paper presents a method for predicting fatigue crack propagation in adhesive bonded composite joints with an initial full-width disbond using finite element analysis and numerical integration of the material's fatigue crack growth rate law. Fatigue tests were conducted on single lap joints. Crack lengths were monitored from four runout corners. In-situ crack growth measurements were performed by ink injection to identify the crack front profile during fatigue loading. The crack growth was modelled using a fracture mechanics criterion considering two different crack propagation patterns. The material's fatigue crack growth rate law was determined experimentally using the standard double cantilever beam and end notch flexure specimens. Using the total strain energy release rate and the two crack scenarios, the numerical model predicted the lower and upper bounds of the measured fatigue crack growth rates of the lap joint.

Keywords: single lap joints; adhesive bond; finite element analysis; fatigue crack growth rate; fatigue life prediction

1. Introduction

The integrity of composite structures subjected to cyclic loads is often limited by the fatigue behaviour of the joints within the structure. Many composite structures use adhesive bonded joints to reduce weight and eliminate the stress concentration that are associated with mechanically fastened joints using bolts or rivets. Narrow lap joints (e.g. 25 mm wide) are often employed in laboratories to investigate the strength and fracture properties under the static and fatigue loads [1, 2]. In recent decades, considerable research has been devoted to predicting the fatigue life in adhesive bonded joints using strength-based and fracture mechanics approaches. In the published literature, investigations into the fatigue behaviour of bonded joints fall into two main categories: one is based on the traditional fatigue design approach, using the *S-N* data to evaluate the load-life relationship [3]; the other is based on the fracture mechanics principles to analyse the crack growth phase [4]. In the latter case, crack propagation rate is usually calculated as the function of the Strain Energy Release Rate (SERR).

In terms of modelling and prediction, Abdel et al. [5] described a procedure based on a fracture mechanics approach to predict the fatigue life of bonded composite joints, i.e. the single lap joint (SLJ) and double lap joint (DLJ). The double cantilever beam (DCB) geometry was used to generate

the material's crack growth rate law. Both the total SERR and mode I SERR were obtained using the Virtual Crack Closure Technique (VCCT) in Finite Element Analysis (FEA). Fatigue life was calculated by integrating the fatigue crack growth rate law between the initial and final crack lengths. The predicted life was in reasonably good agreement with the experimental results. Following the same method, Quaresimin et al. [6] used the total SERR to evaluate the crack propagation phase for a composite single lap joint. Bernasconi et al. [7] predicted the fatigue life based on the equivalent SERR of a composite single lap joint using the mode I crack growth rate law. Using the mode I crack growth rate data has been shown to predict the initial stage of the crack propagation, while the total SERR allowed for a more accurate prediction of the total fatigue crack growth life for a relatively thick composite joint (i.e. 10 mm). Cheuk et al. [8] also used the equivalent SERR to account for the mode ratio effect to investigate fatigue crack propagation behaviour of a metal-to-composite double-lap joint.

A shortcoming of published studies for fatigue life predictions is that only the mode I fracture has been used to determine the material's fatigue crack growth rate law parameters. In fact, other fracture modes also play a role in crack propagation in bonded joints, for example a mode II dominant failure was demonstrated in single lap joints in [5, 6]. Furthermore, significant differences were observed in fatigue delamination growth rate between the mode I and mode II loading [9-12]. Thus, to obtain a theoretically robust and accurate prediction of the mixed mode behaviour of bonded joints, mixed mode fatigue crack growth rate data of the adhesive material and representation of mixed load crack driving force should be employed.

This study investigates the fatigue crack propagation in a single lap bonded joint that contains an initial disbond in the adherend-adhesive interface to mimic the process-induced defects that can arise due to incomplete cure or improper surface treatment. It is reasonable to assume such initial disbond damage, because the single lap joint configuration experiences high interlaminar shear stresses in the adhesive at the bond overlap ends and the interlaminar tensile and shear strengths are very low. Fatigue crack propagation rate in the adhesive was measured by testing the double cantilever beam (DCB) and end notch flexure (ENF) specimens and also data from reference [9] with the same adhesive. Part way through the cyclic test, red ink was injected through a needle nozzle so that the crack front profile at final failure of the specimen could be observed. The novelty aspect of the current work is life prediction combining finite element analysis (FEA) of mixed mode SERR and material's Paris law, which has enabled a better understanding and assessment of fatigue life for realistic joints with defects arising from manufacturing process.

2. Experimental

2.1 Materials and Specimen

Composite adherends were manufactured from a 2 mm-thick laminate made of unidirectional Hexcel® 8552/IM7 pre-preg. The longitudinal (E_L), transverse (E_T) and shear (G_{LT}) elastic moduli of the unidirectional material are 163 GPa, 12 GPa and 5.95 GPa, respectively, with a Poisson's ratio of 0.32 taken from data presented in the material specifications [13]. The test specimens were manually laid up with a quasi-isotropic stacking sequence of $[0/45/90/-45]_S$, and cured in an autoclave. A layer of peel ply was applied to the composite panel during the curing procedure to provide a contaminant free surface. The two "laps" that comprise the sample joint adherends were then cut from the laminate panel using abrasive water jet cutting. The geometry and dimensions of the standard joint with full-width disbond is shown in Figure 1a. Prior to bonding, the Onto™ SB1050 treatment was applied to the 25×25 mm^2 overlap region with a curing stage of 110-130 ºC for 30 minutes to introduce chemical bonding interactions [14]. The Onto™ materials are precursors to highly reactive carbenes, which then reacts and forms a bond to the substrate surface [14]. Cytec FM® 94 modified epoxy adhesive film (a moisture resistant adhesive designed for use in high temperature environments) was used which was assumed to give a nominal bondline thickness of 0.25 mm. The film contains polyester carrier cloth to increase the toughness of bulk adhesive in cohesive failure. A layer of 25 µm thick Teflon® release film in the adherend-adhesive interface was inserted to create the initial disbond damage. Curing of the standard joints was performed in a heating oven at 120 ºC for 40 minutes using a clamping plate with fasteners, at a constant pressure of 0.28 MPa based on ASTM specifications [15]. End tabs of 50 mm length made from identical composite laminate were bonded to the ends of the joints to enable clamping in tests. Four joint runout corners were defined as A, B (the runout end with initial disbond) and C, D (the opposite end without starter crack) for observing cracks, as shown in Figure 1b.

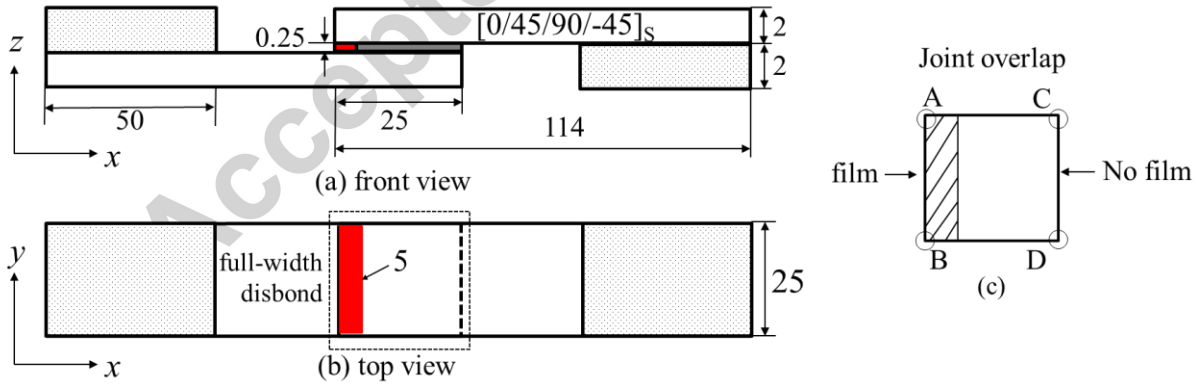

Figure 1 Geometry and dimensions of single lap joint with a full-width initial disbond of 5 mm (unit: mm): (a) front view and (b) top view; (c) enlarged view of joint overlap showing four corners for observing fatigue crack lengths: A and B at the end with an initial disbond, C and D at the opposite end without starter crack.

2.2 Experimental procedure

An Instron 8871 servo-hydraulic testing system with a 10 kN load cell was used to apply cyclic loading to the test specimens. Tests were conducted at the laboratory ambient temperature, using a constant amplitude loading regime. The cyclic load ratio was set to 0.1 and the loading frequency was 3 Hz to avoid the heating effects on the composites. The maximum load applied was 50% of the ultimate tensile failure load (P_{max}=3.58 kN). Fatigue tests were conducted on four specimens, named as F1, F2, F3 and F4 for repeatability.

During the fatigue testing, crack propagation was monitored by observing the bondline and the surrounding material using a travelling microscope equipped with a digital camera with the aid of the scale shown in Fig. 2a. Once the crack was opened (at the maximum fatigue load), red ink was manually injected through a needle nozzle into the bond interface to allow the liquid to flow to the crack front to capture the single crack propagation profile to be captured for a specimen at that stage of the test. This is similar to dye penetrant, which is one of the non-destructive techniques (NDT) used in the aerospace industry and is assumed not to influence the crack propagation [16]. It was found during the first trial (specimen F1) that, due to a spew fillet at the A-B end (with initial disbond), crack initiation took place a considerable time into the test (around 200,000 cycles) rather than straightaway in the separation of the clean film. For other specimens (e.g. F2-F4), the fillet was removed before testing to improve the crack visibility, as the aim of this research is to study the crack propagation phase rather than crack initiation.

2.3 Crack growth profiles

Crack propagation was monitored by measuring crack length from the four corners of the bond overlap, as the stress gradient throughout a bond length is non-uniform and it is the overlap end of a flat bond undergo the highest stress level rather than the central bond area. Figure 2a presents the final failure of specimen F2, which indicates that the propagation of cracks occurred mainly at the adhesive-adherend interface (adhesion failure), which is attributed to the existing carrier cloth in the adhesive which has toughened the bulk via introduction of crack arresting mechanism. The yellow colour line follows the crack path where the lead crack and secondary crack met in the centre of the overlap. No failure in composites (adherends) was observed. Figures 2b is a schematic marking the locations in Figure 2c and 2d showing cracks propagating from both overlap ends. Photos were taken with a 40X optical microscope from corners A and C (the arrows and yellow line indicate the crack propagation path). The two cracks propagated toward the joint centre and joined after a certain number of load cycles.

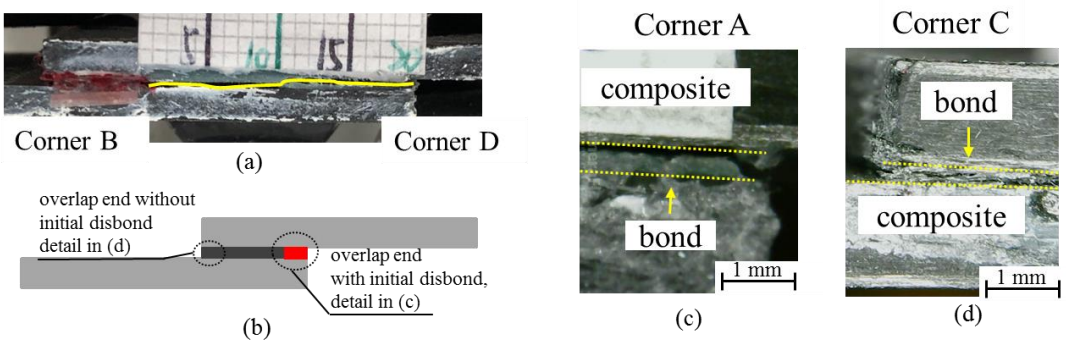

Figure 2 (a) Crack paths at failure of specimen F2, (b) Schematic drawing indicating the two crack propagation sites observed from (c) corner A and (d) corner C in specimen F1

At final failure, the bond had completely failed and the specimen had separated into two parts in adhesion failure for all specimens (see fracture surfaces in Figure 4). The red ink which had dried on the two faces at the intermediate stage of the test could then be observed to show the crack propagation profile at that point during the test. The left red interface in Figure 3a indicates the crack front at 151,360 cycles for specimen F2. Four positions (I, II, III, IV) were chosen to measure the instantaneous crack lengths under microscope. It is verified that the crack lengths at the selected four locations are approximately identical, indicating a uniform crack front during the propagation phase. Another trial was performed to insert the red ink to both sides of the specimen F4 at 186,386 cycles, to prove the crack propagation from two runout sides (Figure 3b). The red ink showed that the cracks from both sides propagated in almost the same pattern and (although sensitive to the bond quality and adhesive thickness) the crack front profile was roughly uniform as the stress gradient throughout a bond width is almost uniform.

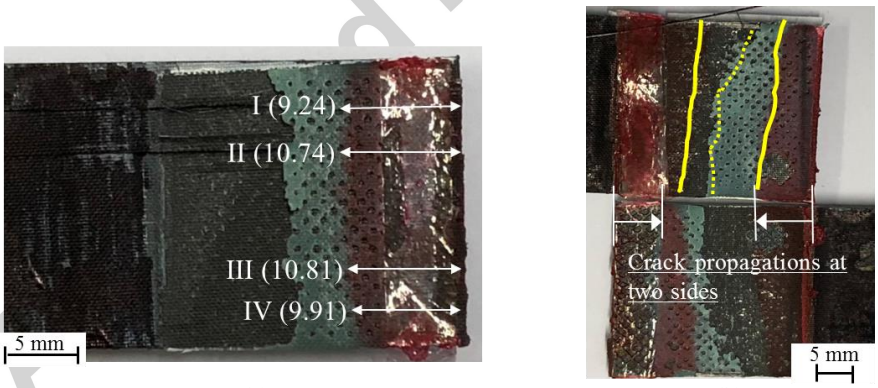

Figure 3 Post failure observations of (a) specimen F2, red ink shows the crack front at 151,360 cycles, (b) specimen F4, red ink was injected from both sides of overlap ends at 186,386 cycles.

2.4 Fatigue crack growth life

Figure 4 shows the monitored crack lengths (a) measured from four points versus number of cycles (N) of four specimens: F1, F2, F3, F4. Crack propagation was not uniform, and non-symmetric profiles were observed.

For specimen F1, the crack was initially observed only at corners A and B, although their start point was slightly different. After about 200,000 cycles, cracks were also detected at corners C and D due to the secondary bending effect resulting in a high stress which caused the adhesive fillet to degrade and fail. F1 withstood many more cycles to failure than others. This is because F1 had fillets of adhesive at the ends of the lap, which reduced stress concentrations and hindered crack initiation.

For the other three specimens (F2-F4), cracks were found to have propagated from all the four corners from the initial fatigue cycles. This is different to the crack propagation observed in F1 because the adhesive fillet has been removed before conducting fatigue tests on the later specimens. The crack growth rate (i.e. the gradient of *a*-*N* curves) was approximately the same for corners A and B, and also the same for corners C and D (although at a different rate to corners A and B). In conjunction with post-failure examination of the pattern of injected red ink, this observation of similar crack growth rates as corners A and B, and corners C and D supports our assertion of a uniform crack front. Test F3 experienced much faster crack propagation rate due to peculiar interface surfaces (Figure 4c) which might be arisen from anomalies in the manufacturing process (e.g. size tolerance and adhesive chemistry), particularly noting that even macroscopically identical specimens can have significant scatter in experimental fatigue tests. This leads to the crack propagation concentrating more at one end of the lap joint rather than proceeding equally from both ends. However, these scenarios are common in the aerospace bonding applications, which is the reason why regulators ask for continued safe flight even with a bonded repair that has completely failed in AC20-107B/AMC20-29 [17] as the bonding quality was not assured.

Calculations of SERR require a value for "crack length", which obviously poses some issues when considering non-uniform cracks. Two possibilities were considered: the crack averaged from the measures taken from the corners with an artificial defect side (average of corners A and B, defined as lead crack, a_1), and the average crack emerged from the runout without initial crack starter due to fatigue cycles (average of corners C and D, defined as secondary crack, a_2). Figure 5 plots crack propagation life for the four specimens calculated from both (a) a_1 and (b) a_2. It could be seen that F3 experiences a very fast crack propagation due to an apparent observed instantaneous interface failure (see Figure 4c) and weak bond fracture surface which might have been induced by surface contaminants (possibly arising from non-uniform application of the Onto surface treatment) or adhesive chemistry or curing processing procedure. The adhesive and adherend interface clearly has a large influence on the fatigue behaviour of the single lap joint.

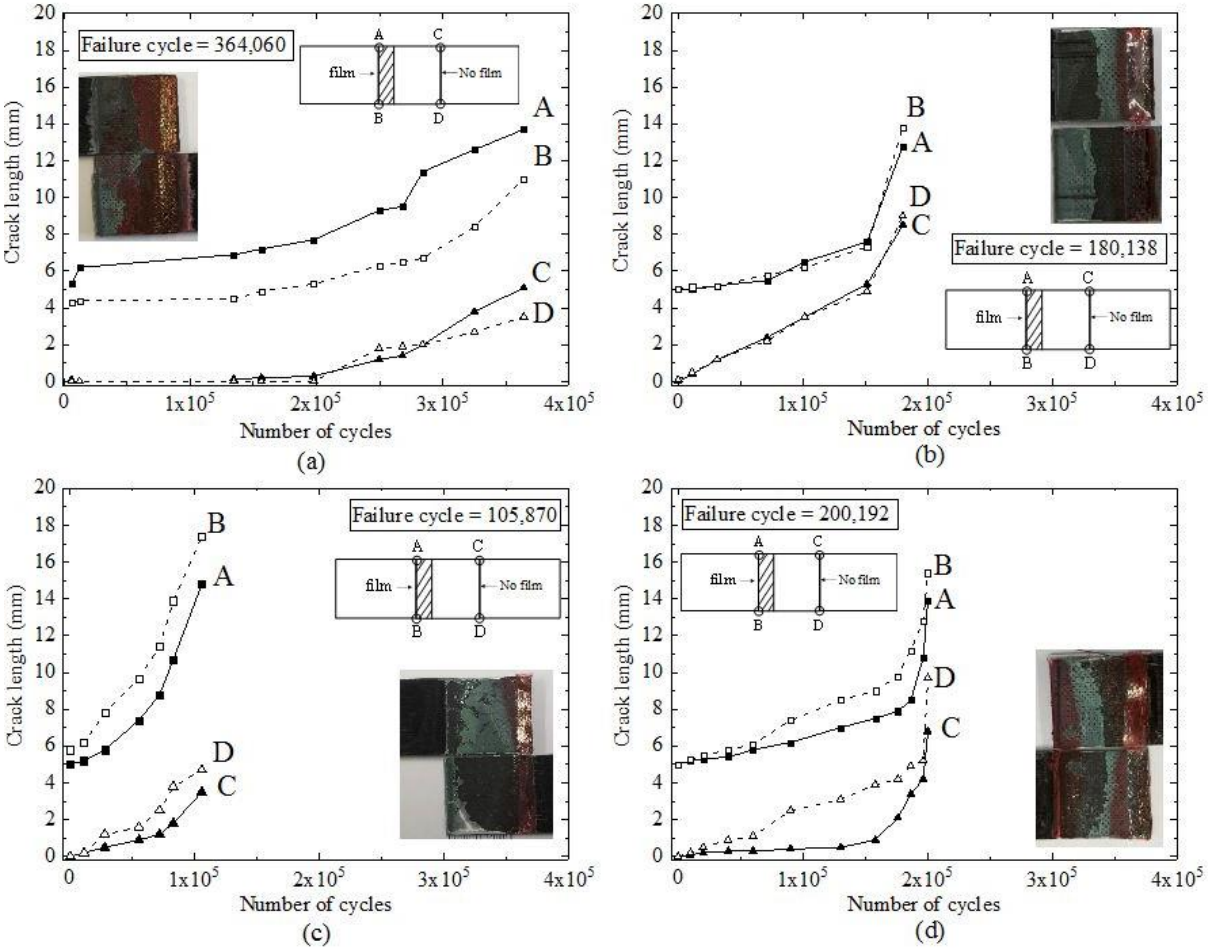

Figure 4 Measured crack length versus cycle numbers, (a) specimen F1 (N_f =364,060 cycles), (b) F2 (N_f =180,138 cycles), (c) F3 (N_f =105,870 cycles), (d) F4 (N_f =200,192 cycles); faster crack growth was observed from corners A and B (referring to Figure 1b).

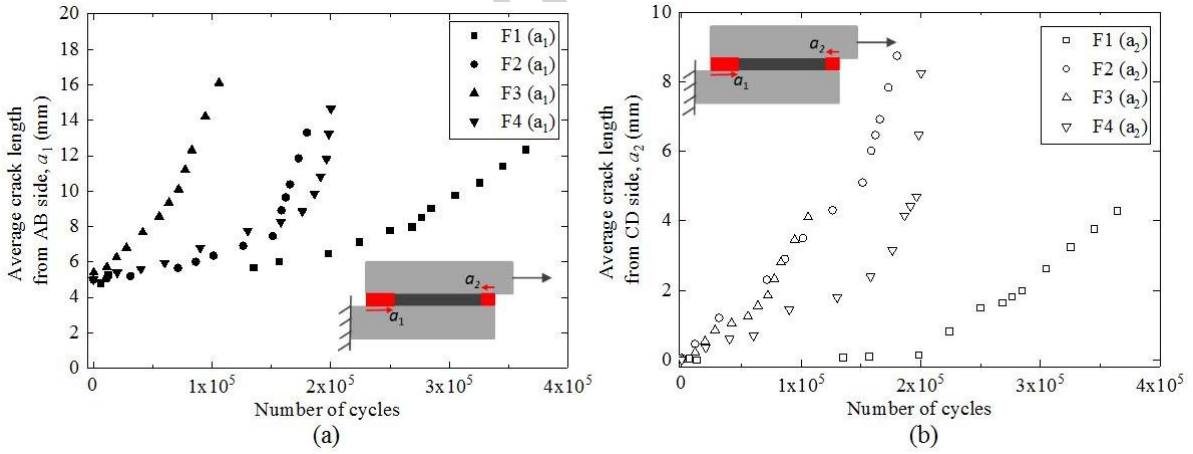

Figure 5 Fatigue crack growth life for the single lap joints based on (a) lead crack length from corners A and B (a_1), and (b) secondary crack length from corners C and D (a_2)

2.5 Fatigue crack growth rate (FCGR)

Determining crack length by eye can result in errors, (e.g. missing the first crack initiation point in the *a-N* curve) which can induce a significant effect on the *a-N* plots. Fatigue crack growth rate (FCGR) is therefore used as a more robust indicator of crack growth behaviour. FCGR was calculated from the

experimentally obtained *a-N* curves using the 7-point incremental polynominal method, specified by ASTM E647 [18].

Figure 4 showed that a_1 (AB side) is always larger than a_2 (CD side) and the crack growth rates at AB side and CD side are almost similar (the rates are slightly quicker at CD for F2 related to the bond quality). Therefore, the lead crack length a_1 was used in calculating the crack growth rate, since it is the dominant crack (developed from the initial disbond). Figure 6 illustrates the crack growth rate of single lap joints. It can be seen that the initial crack growth increment of 1 mm (from the 5 mm initial disbond to 6 mm) is not covered. Although this early disbond growth is of practical interest, it is very difficult to observe this minor crack length at the initial stage, which is acknowledged as a limitation of the experimental procedure. It should also be noted from Figure 6 that the differences in FCGR of specimen F1 and other specimens are significant, due to the differences between the *a-N* curves of these specimens. For instance, Figure 5a shows that crack growth in F1 is very gradual compared to the results for F2 and F4 which show a rapid increase in FCGR at around 200,000 cycles. Consequently, F1 has a much longer fatigue life as it shows the effect of the fillet in hindering crack initiation and growth (by comparing *a-N* curves with F2-F4). Test F3 experienced much faster crack propagation due to interface surface quality (Fig. 4c) which might be arisen from anomalies in the manufacturing process (e.g. size tolerance and adhesive chemistry). Although specimen F1 is geometrically slightly different at the initial cycles from the other three specimens (the adhesive fillet was removed in F2-F4), the results for F1 are still included in calculations of FCGR in crack propagation phase, as FCGR is related to the stage where crack has already propagated.

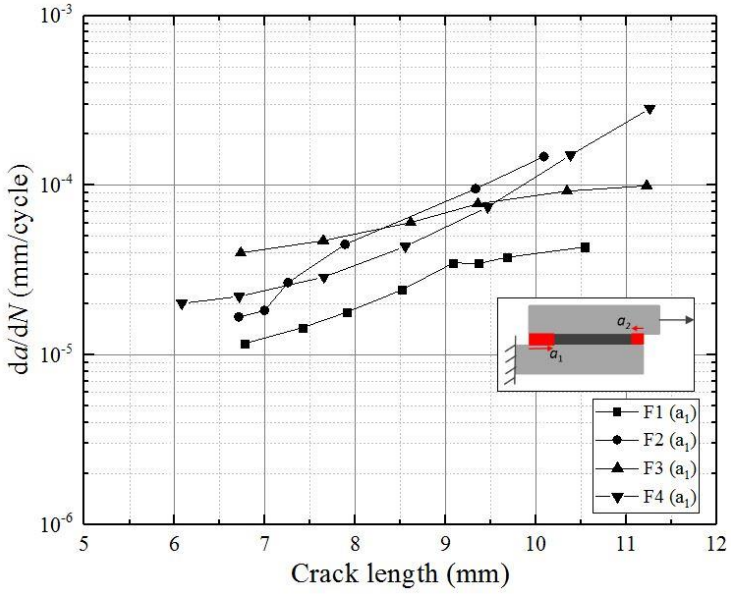

Figure 6 Fatigue crack growth rate (FCGR) calculated from the *a* vs. *N* relation using the lead crack length, a_1

3. Modelling and life prediction

3.1 Finite element based models

The FE modelling work was carried out in the ABAQUS/CAE code 6.14 Package. The models of lap joints follow the actual specimen geometry and dimensions (excluding the tabbed area), as illustrated in Figure 1a. The elastic properties of the quasi-isotropic laminate and adhesive used in the finite element model are summarised in Table 1. The adherend elastic properties were calculated using the laminate theory and the adhesive properties were taken from the data provided in [9].

Table 1 Elastic properties of adherends and adhesive

	E_x (GPa)	E_y (GPa)	ν_{xy}	G_{xy} (GPa)
Adherend 8552/IM7 ($[0/45/90/-45]_S$)	63.17	63.17	0.32	14.08
Adhesive FM94 [9]	3	3	0.3	1.15

A 2D plane strain finite element model was used to reduce the computational expense. For lap joints with full-width initial disbond, experimental observations found no significant variations in crack length across the width of the specimen and it is therefore reasonable assume a uniform crack front and to analyse the crack propagation problem with 2D plane strain elements. Figure 7 shows the 2D finite element model of the single lap joint, with details of the initial crack geometry. For a more complete understanding of the joint behaviour, two modelling scenarios have been taken into account:

(1) the first case considers only lead crack length a_1, ignoring the contribution of secondary crack length a_2. (Based on the observation crack growth in specimen F3, cracks from C&D sides were insignificant compared to the cracks from A&B) ;

(2) the other case considers lead crack length a_1 under the influence of secondary crack length a_2, which is more representative of the actual behaviour. The change of crack length a_2 in the model is set to a_1 according to the SERR ratio calculated at the crack tips of a_1 and a_2.

All the modelling work was based on the adhesion failure suggested by the experimental results. The crack tip SERR was obtained from the VCCT method. Boundary conditions were applied such that the displacement of all the nodes at one end was restrained in the *x* and *y* directions, whilst those at the other end were restrained in the *y* direction only and the maximum cyclic load P_{max} in the fatigue testing was applied in the *x* direction. A refined mesh was used at the interface corner (0.5×0.5 mm^2 based on a mesh sensitivity study) as it experiences the highest stress (and stress gradients) and therefore a smaller mesh size necessary to capture the rapid change in stress and energy release during crack propagation at this location with sufficient accuracy. A tie constraint was defined at the interface between the bottom adherend and the adhesive, which allowed the nodes of the respective surfaces to have coupled behaviour with identical motion. For the disbond, a contact interaction is defined between the top adherend and the adhesive with the bonded area restricted to a certain region (which

excludes the pre-crack). The FE analysis was conducted with geometric non-linearity to capture the effects of out-of-plane-bending.

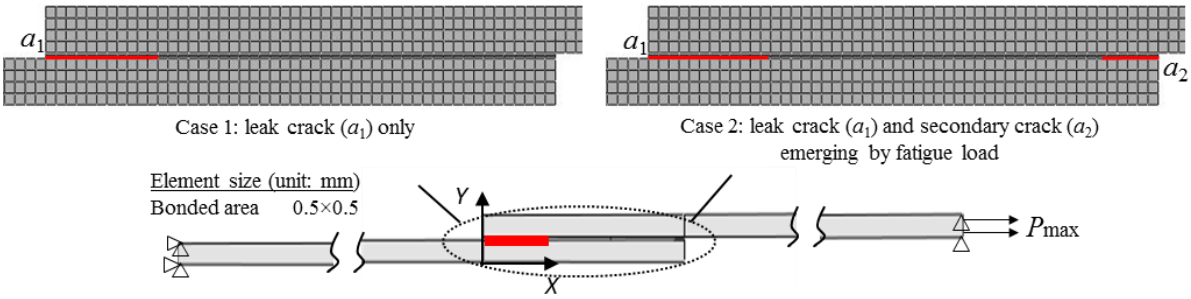

Figure 7 Finite element model of the joint and mesh details at the bond overlap region; two scenarios were assumed: Case 1 considers only the lead crack a_1 propagating from the initial disbond; Case 2 reflects lead crack a_1 under the influence of a secondary crack a_2; mesh size is 0.5 x 0.5 mm^2 based on a mesh sensitivity study.

3.2 Calculation of SERR

The total SERR was employed for the crack growth integration, since for the relatively thin adherends (e.g. 2 mm) the total SERR and equivalent SERR were shown to provide similar predictions [19]. Figure 8a compares the calculated SERR components, G_I and G_{II}, under quasi-static load, for both cases obtained from FEA:

(1) lead crack a_1 alone, and

(2) lead crack a_1 under the influence of secondary crack a_2.

Figure 8b presents the calculated total SERR considering these two cases. For both cases, it can be seen that mode II gives the greater strain energy release, but that the contribution of mode I is not negligible (particularly during the initial stages). However, there are significant differences in how the SERR varies with crack length for Case 1 and Case 2.

For case 1, it can be seen that both mode I and mode II increase as the crack grows, but that at larger crack lengths, mode II SERR increases significantly due to the geometric non-linearity resulting from the large bending moment effect. As the crack propagates to the end, mode I decreases and mode II increases suddenly to failure.

For case 2, mode II SERR increases from both runouts up to a maximum value halfway along the joint overlap, while mode I SERR reaches its lowest value at the same point as the cracks propagates from both runout ends.

In terms of SERRs, case 2 seems to be more appropriate to describe the general conditions of the propagation while case 1 defines a more conservative scenario which could result in a longer predicted fatigue life. It can be concluded that for lap joint configuration, the total crack length grows faster if

cracks grow from both sides of the lap joint than if a crack grows from just one one side of the lap joint.

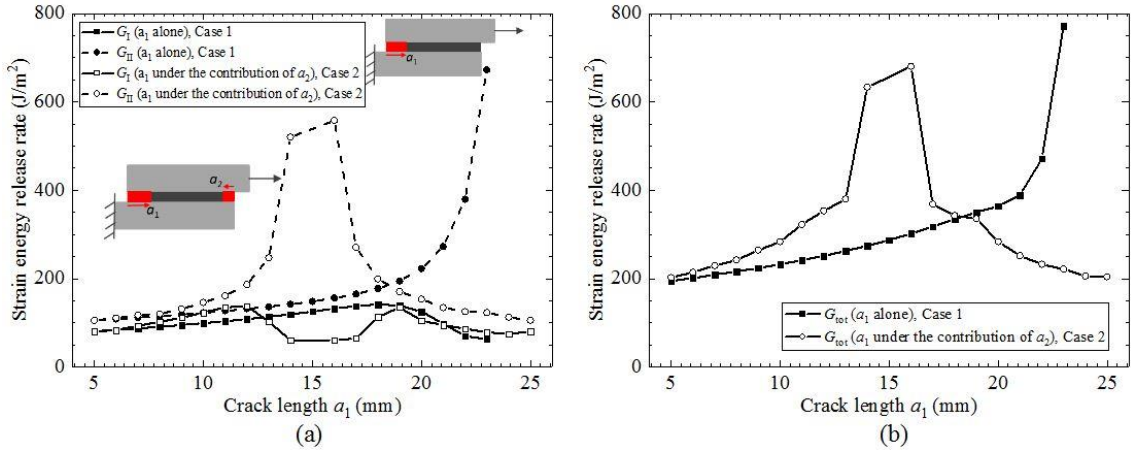

Figure 8 (a) Calculated mode I and mode II SERR components in case 1 and case 2, G_I and G_{II} are at maximum cyclic load, (b) Comparison of total SERR between the case 1 and case 2

The mixed mode ratio is important as the joints experience mixed mode load during the entire fatigue life. The mode-mixity ratios are defined in Eq. (1) and Eq. (2), by dividing the mode I or mode II SERR component by the total SERR. Figure 9 plots the calculated mode-mixity ratio (ψ_1 and ψ_2) of the lap joint considering (a) a_1 only and (b) a_1 under influence of a_2 based on the results in Figure 8. The mode-mixity ratios are approximately 0.5 during most of the fatigue life of the joint (i.e. as the crack length propagated from 5 mm to about 17 mm). The contribution of mode II becomes more important as the crack propagates along the overlap length, at which the crack propagation becomes unstable and the specimens suddenly fail. Thus, the relative contribution of the mode I and mode II components to the crack propagation is continuously changing at the final stage.

$$\psi_1 = \frac{G_I}{G_T} = \frac{G_I}{G_I + G_{II}} \quad \textbf{(1)}$$

$$\psi_2 = \frac{G_{II}}{G_T} = \frac{G_{II}}{G_I + G_{II}} \quad \textbf{(2)}$$

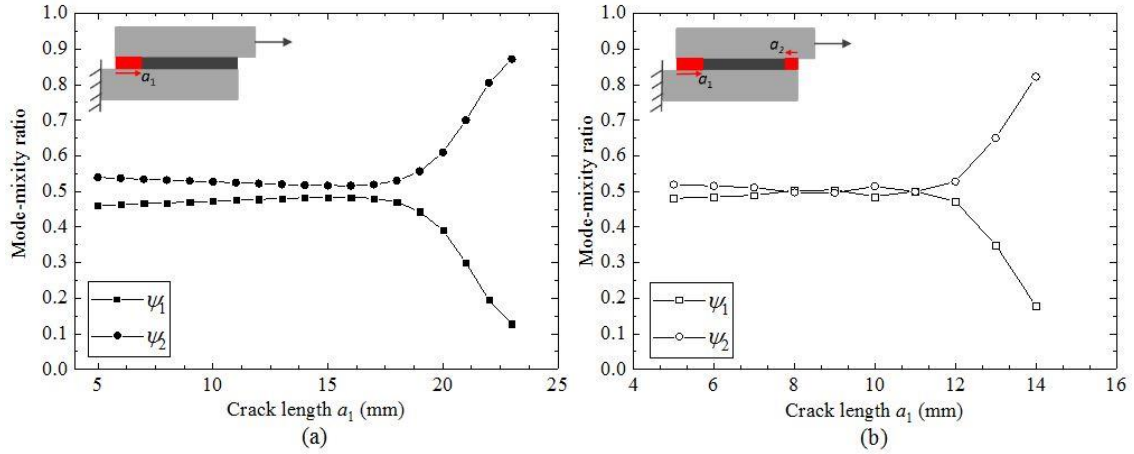

Figure 9 Mode-mixity ratios (ψ_1 and ψ_2) of lap joint in adhesion failure considering (a) a_1 only and (b) a_1 under influence of a_2

3.3 Fatigue life prediction

The Paris law (Eq. (3)) describes fatigue crack growth rate as a function of the SERR by correlating experimental data with two material constants C and m. It was originally developed for cracks in composite materials and is also used for predicting fatigue life for bonded joints [20]. The use of G_{max} in the traditional Paris law has been challenged in [21, 22]. A lack of similitude with G_{max} can result in trends being incorrectly attributed to test variables such as the applied stress ratio and residual stress [21]. In addition, the value range of the Paris law exponent (m) is much higher for FCG rate curves of composite laminates, which can lead to large uncertainties in the predicted delamination growth rate [22]. Therefore, the use of $\sqrt{G}$ or the Hartman-Schijve relation was proposed for similitude to improve the prediction of fatigue delamination growth rate as it significantly reduces the value of the exponent [22]. However, these studies were focused on the fatigue delamination within composite laminates rather than disbond in adhesives. Martin and Murri [23] has found that for mode I cracks, the exponent ranges from 6.1 to 10.5 for composite laminates, indicating a relatively steeper slope of the FCG rate curve; however, the experimental tests in this study have found the exponent for mode I FCG rate in adhesive FM94 being around 4.5 to 6 (see Figure 10 and Table 2, and 2.5 to 5 for FM73 adhesive in [24]) and the FCG rate curves are much less steep than that of composite laminates (due to the relative brittleness of epoxy resin in a composite laminate when compared to the relative ductility of an adhesive). Therefore, in this study, the Paris law based on G_{max}, Eq. (3), is applied for the prediction, which has already been successfully applied to the mixed mode behaviour of adhesive joints in [10]. In Figure 10, a good correlation of mode I data and separation of the mode I and mode II test data of the adhesive is clearly demonstrated. Integrating Eq. (3) leads to the cycle numbers required to propagate the initial crack to critical crack length, Eq. (4).

$$\frac{da}{dN} = C(G_{max})^m \tag{3}$$

$$N_p = \int_0^{N_p} dN = \int_{a_0}^{a_f} \frac{da}{C(G_{max})^m} \tag{4}$$

where G_{max} used in this study is $G_{tot,\ max}$, and the values of the Paris law parameters C and m are determined from the experimental data.

In determining the crack growth rate law, a DCB (mode I) and ENF (mode II) geometry made with 8552/AS7 prepreg in a quasi-isotropic layup of $[0/45/90/-45]_{2S}$ bonded with FM94 adhesive were tested in the experimental programme. Schematic of DCB and ENF specimens is shown in Figure 10. The fatigue tests were conducted at a frequency of 5 Hz under displacement control and the stress ratio was 0.1. In analysing the DCB and ENF results, the SERR was calculated from experimental compliance and the FCGR was deduced from the a vs. N relation using 7-point polynomial method in the ASTM standard [19].

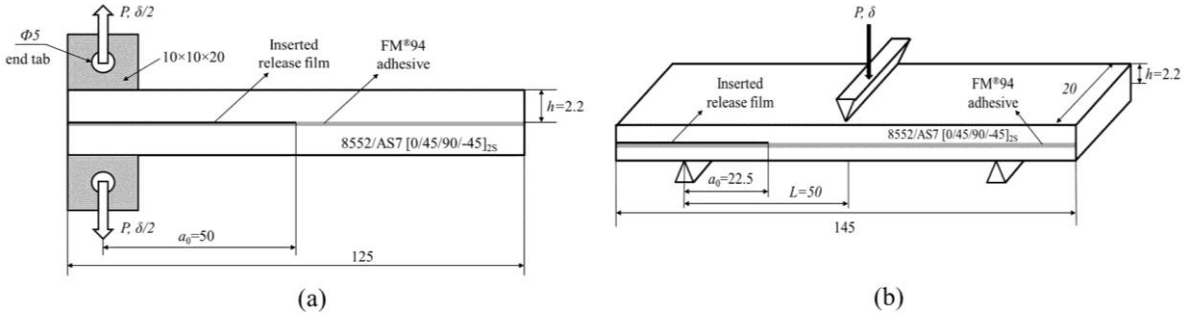

Figure 10 Geometry, materials and layup of (a) DCB and (b) ENF specimens in determining the fatigue disbond growth rate (unit: mm)

In [9], fatigue tests were conducted on the FM94 adhesive bonded with aluminium substrates under the mode I and mode II loading, and also under mixed mode of 25% and 75%. Figure 11 shows the variation of crack growth rate (da/dN) with maximum SERR (G_{max}) for the fatigue test. Two groups of data were found in Figure 11: one comprises mode I and all mixed modes apart from pure mode II, the other group contains pure mode II results. It is interesting to note that mixed mode tests containing 25% and 75% of mode II have similar growth rates to those found in pure mode I tests when expressed in terms of maximum SERR ($G_{tot,max} = G_{I,\,max} + G_{II,max}$). This is influenced by the presence of fibre carrier cloth in this adhesive that can bear the mode II loads. This trend is similar to previous work in [11, 12] with different composite materials, where results for mode I and mixed mode are similar to one another, but markedly different from pure mode II rate. The average fatigue delamination growth rate parameters of various mode ratios in Paris law obtained through delamination fatigue testing and used for fatigue life prediction are listed in Table 2.

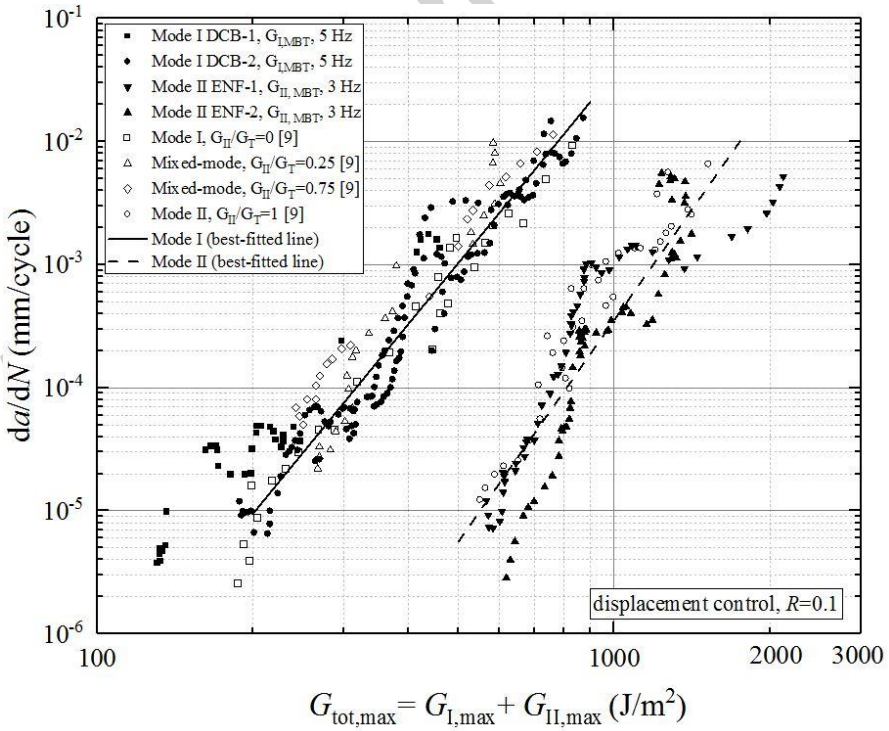

Figure 11 Measured fatigue crack growth rate versus the maximum total SERR for FM94 adhesive under mixed mode cases. Black filled symbols in the left group are DCB adhesion failure (DCB-1) and mixed failure (DCB-2) (this study); in the right group show

ENF adhesion failure (ENF-1, 2); black unfilled symbols indicate the mixed mode and single mode tests taken from [9] in adhesion failure; black solid and dashed lines are the best fitted curves of mode I and mode II test results.

Table 2 Paris law material constants for fatigue disbond growth rate of adhesive FM94 under various mode ratios obtained from tests (Fig. 11) (in mm/cycle, J/m^2 unit)

Mixed mode ratio (ψ_2)	C	log C	m
0 (mode I, best fitted values)	5.75×10^{-17}	-16.24	4.86
0.25	1.91×10^{-20}	-19.72	6.30
0.75	7.24×10^{-15}	-14.14	4.59
1 (mode II, best fitted values)	4.07×10^{-22}	-21.39	5.98

Russell et al. [25] defined a linear rule of mixtures of the individual propagation rates between various mode ratios. Blanco et al. [26] expressed the non-monotonic relationship on the effect of the mixed mode ratio on the fatigue delamination growth rates. It is suggested that the dependency of the Paris law parameters is due to a complex interaction of fibre bridging, matrix cracking and brittle fracture behavior.

Figure 12 shows the calculated Paris law coefficients at various mode ratios. This figure completely interprets the fatigue disbond growth data in Figure 11. It can be seen that the Paris law expression of different failure modes has almost the same trend, that's why the values of the Paris law exponent (m) in Figure 12b are almost identical (from 4.59 to 6.30). However, the Paris law coefficient (log C) is scattered as it indicates the intersection of the disbond growth data with the da/dN axis. The material constants for mode-mixity (ψ_2) of 0.25 and 0.75 were taken from literature [9], there might be some possibilities of fabrication and bonding issues that makes the point slightly away from the fitting curve. However, these mixed mode data are necessary as they indicate the particular behaviour of fatigue disbond growth rate of this adhesive, which is not the case for the other adhesives, such as FM73. Although the small sample size limits the robustness of the conclusions that can be drawn regarding variations of Paris law coefficients under mixed mode loading, a linear fit curve is used to interpolate the relationship of coefficients and exponents with the mixed mode ratio. Extensive experimental testing to generate a robust data set is a clear requirement to underpin further work in this area.

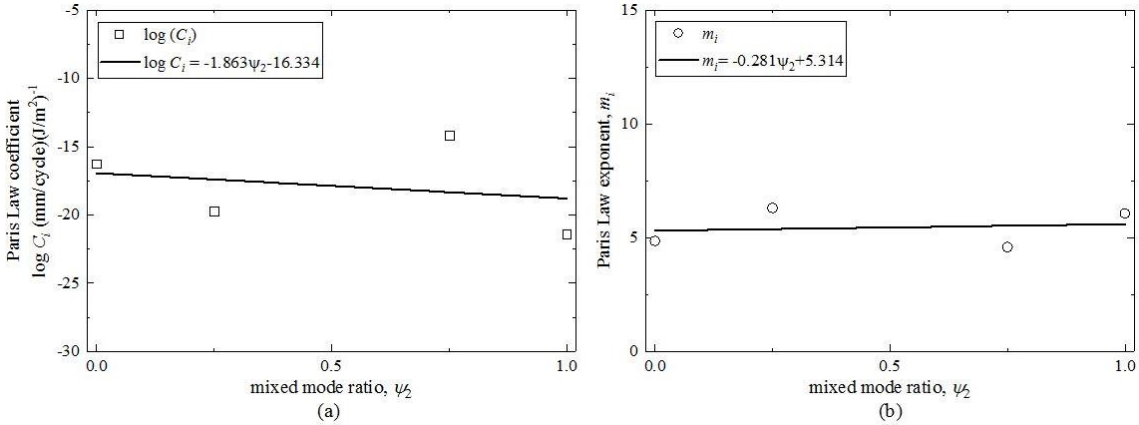

Figure 12 Linear fit curves of (a) the coefficient and (b) the exponent in the Paris law vs. the mixed mode ratio, log C_i = -1.86Ψ_2 -16.33, m_i = -0.28Ψ_2 +5.31

3.4 Prediction vs. test results: model validation

Predicted fatigue life was obtained by numerical integration of the Paris law using Eq. (4). The crack propagation can be artificially divided into many integration segments, such as, crack extension from 5 to 6 mm. When the integration segment is sufficiently small, the crack growth rate during this crack growth period can be assumed to be constant. Therefore, by inputting the mixed mode material data and the calculated SERR values, the fatigue life of certain crack growth period can be calculated by the integration. For the entire fatigue life, the lower limit of integration a_0 is the initial crack length at the beginning of the propagation, which is 5 mm in this study, and the upper limit is the total joint failure, i.e., $G_{tot} > G_{critical}$. Figure 13 shows the fatigue life prediction obtained by the models based on the total life results considering cracks either from one runout end (a_1 only) or both runout ends (a_1 under influence of a_2). Note that for consistency, a_1 is used as the dominant crack length in the da/dN plots.

It can be seen from the modelling results that the initial crack growth rate is slow (due to the small SERR values) and cracks propagate slowly. As the number of cycles accumulates, the crack begins to propagate faster with the increasing SERR values, followed by a sudden failure. The fatigue life obtained with the prediction growth of a_1 without the influence of a_2 forms a lower bound to the experimental results for crack growth (and correlates well with the data from specimen F1). The fatigue life obtained with the prediction growth of a_1 under influence of a_2 keeps increasing and developing between F2 and F3, resulting in a fatigue life prediction that is more realistic in most cases. In general, the experimental data are within the prediction bound except F3, which grew faster and failed in a very short life (see fracture surface in Figure 4c). This comparison has successfully demonstrated the applicability of the prediction models, which can cover the scatters in the fatigue tests.

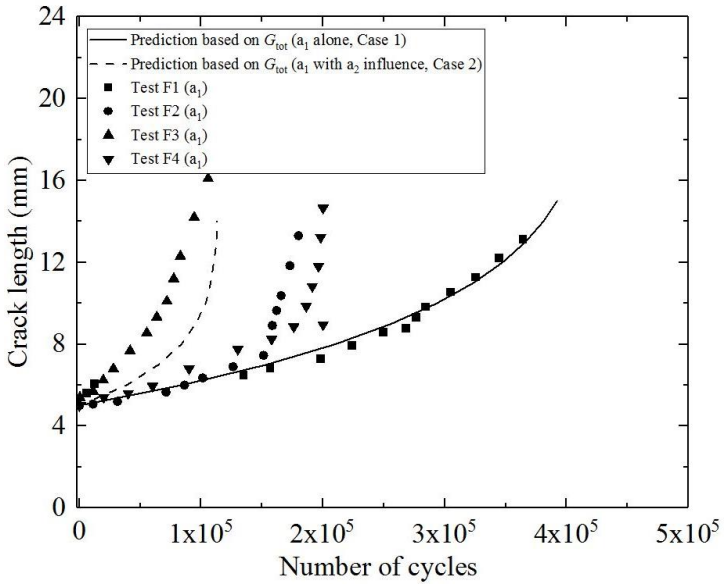

Figure 13 Fatigue life predictions based on the G_{tot} parameter for fatigue tests considering lead crack from initial disbond (a_1 only) and the two crack scenario (a_1 under influence of a_2) and comparison with experimental test results.

Figure 14 shows fatigue crack propagation rate (da/dN) against crack length (a_1) based on the G_{tot} parameters from both modelling (lines) and experiments (data points). The use of da/dN vs. a curves is to eliminate the potential large errors in predicted fatigue life which would be introduced if the first prediction point in the a-N curve was inaccurate. The predicted da/dN covers almost half decade of the legend (from 2×10^{-5} to 6×10^{-5}) at the initial crack length, indicating the significant influence of another cracks a_2 occurring due to fatigue load history. Cracks from both sides (a_1 under influence of a_2) propagated faster than one dominant crack from one side (a_1 only). The experimental results of FCGR data of the joints are all within the range of the FE modelling prediction (the lower and upper bound are covered), which demonstrates the predictive capabilities of the FCGR approach.

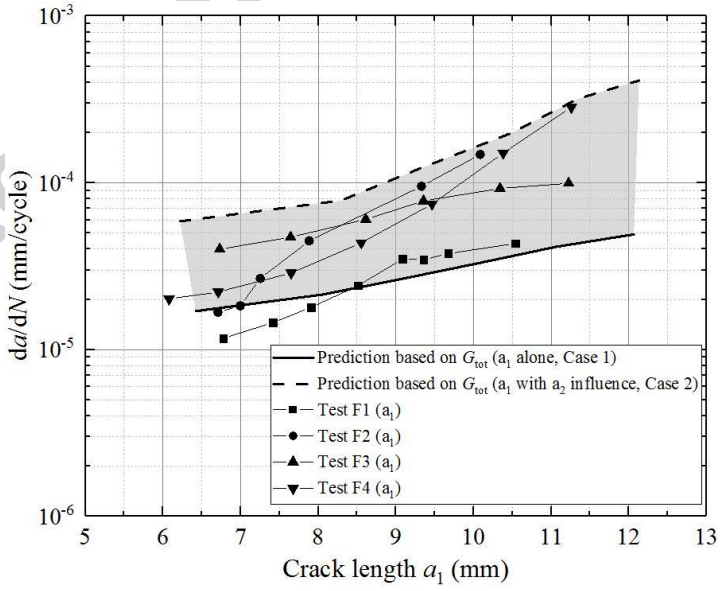

Figure 14 Comparison of predicted fatigue crack growth rates (calculated from crack propagation life curves in Figure 13) and comparison with experimental tests

4. Conclusions

Crack growth behaviour in adhesive bonded lap joints was modelled and fatigue crack propagation life was predicted based on finite element calculated strain energy release rates and numerical integration of the material's fatigue crack propagation rate data from single mode and mixed mode tests. The following conclusions are drawn:

1. In fatigue tests, although the initial disbond was located at one end of the overlap, a second crack initiated and propagated from the opposite end owing to high interlaminar stresses at the joint runout. With the aid of injected red ink, the crack propagation front was observed showing an approximately uniform profile.
2. Using mixed mode fatigue crack growth rate data is necessary as the disbond cracks in the lap joints were subjected to mixed mode conditions.
3. In addition to the lead crack propagation from the initial disbond, the initiation and propagation of a second crack from the opposite end of the joint overlap was also modelled. Predicted crack growth life is longer than the test result (i.e. non-conservative prediction) if only considering the dominant crack propagating from the initial disbond, whilst the predicted life is shorter if crack propagation from both runout ends representing a more severe crack growth scenario. These two possibilities provide the upper and lower bounds in the predicted fatigue crack growth rate and cover the variations and scatters found in the experimental test results.

Acknowledgement

This research is funded by Coventry University, Faculty of Engineering, Environment and Computing, through a PhD studentship to Yiding Liu.

References

[1] Ribeiro F, Campilho RDSG, Carbas R, da Silva LFM. Strength and damage growth in composite bonded joints with defects. Compos Part B Eng 2016;100:91–100.
[2] Olajide S, Kandare E, Khatibi A. Fatigue life uncertainty of adhesively bonded composite scarf joints – an airworthiness perspective. J Adhes 2017;93:515–30.
[3] Ishii K, Imanaka M, Nakayama H, Kodama H. Evaluation of the fatigue strength of adhesively bonded CFRP/metal single and single-step double-lap joints. Compos Sci Technol 1999;59:1675–83.
[4] Hadavinia H, Kinloch AJ, Little MSG, Taylor AC. The prediction of crack growth in bonded joints under cyclic-fatigue loading II. Analytical and finite element studies. Int J Adhes Adhes 2003;23:463–71.
[5] Abdel Wahab MM, Ashcroft IA, Crocombe AD, Smith P. Finite element prediction of fatigue crack propagation lifetime in composite bonded joints. Compos Part A 2004;35:213–22.
[6] Quaresimin M, Ricotta M. Fatigue behaviour and damage evolution of single lap bonded joints in composite material. Compos Sci Technol 2006;66:176–87.
[7] Bernasconi A, Jamil A, Moroni F, Pirondi A. A study on fatigue crack propagation in thick composite adhesively bonded joints. Int J Fatigue 2013;50:18–25.
[8] Cheuk P, Tong L, Wang C, Baker A, Chalkley P. Fatigue crack growth in adhesively bonded composite-metal double-lap joints. Compos Struct 2002;57:109–15.
[9] Doucet J. Fatigue life enhancement of aircraft structures through bonded crack retarders

(BCR). Cranfield Thesis. 2016.
[10] Kenane M, Benzeggagh M. Mixed-mode delamination fracture toughness of unidirectional glass/epoxy composites under fatigue loading. Compos Sci Technol 1997;57:597–605.
[11] Benzeggagh M, Kenane M. Measurement of mixed-mode delamination fracture toughness of unidirectional glass/epoxy composites with mixed-mode bending apparatus. Compos Sci Technol 1996;56:439–49.
[12] Zhang JY, Peng L, Zhao LB, Fei B. Fatigue delamination growth rates and thresholds of composite laminates under mixed mode loading. Int J Fatigue 2012;40:7–15
[13] Hexcel. HexPly ® 8552 - Product Data Sheet - EU Version 2016:1–6.
[14] Oxford advanced Surface. Onto™ SB1050 : Adhesion promotion of polyurethane and epoxy adhesives. 2015.
[15] ASTM D5868. Standard test method for lap shear adhesion for fiber reinforced plastic (FRP) 2005;1:4–5.
[16] Cawley P. Non-destructive testing—current capabilities and future directions. Proc Inst Mech Eng Part L J Mater Des Appl 2001;215:213–23.
[17] EASA. Notification of a proposal to issue a certification memorandum sugject bonded repair size limits in accordance with CS 2x . 603 and AMC 20-29. 2014.
[18] ASTM Standard E647−13. Standard test method for measurement of fatigue crack growth rates. ASTM B Stand 2016;3:1–49.
[19] Khoramishad H, Crocombe AD, Katnam KB, Ashcroft IA. Predicting fatigue damage in adhesively bonded joints using a cohesive zone model. Int J Fatigue 2010;32:1146–58.
[20] Pugno N, Ciavarella M, Cornetti P, Carpinteri A. A generalized Paris' law for fatigue crack growth. J Mech Phys Solids 2006;54:1333–49.
[21] Rans C, Alderliesten R, Benedictus R. Misinterpreting the results: How similitude can improve our understanding of fatigue delamination growth. Compos Sci Technol 2011;71:230–8.
[22] Jones R, Kinloch AJ, Michopoulos JG, Brunner AJ, Phan N. Delamination growth in polymer-matrix fibre composites and the use of fracture mechanics data for material characterisation and life prediction. Compos Struct 2017;180:316–33.
[23] Martin RH, Murri GB. Characterization of Mode I and Mode II Delamination Growth and Thresholds in AS4/PEEK Composites. Compos Mater Test Des (Vol 9), ASTM STP 1059 1988:251–70.
[24] Hafiz TA, Abdel Wahab MM, Crocombe AD, Smith PA. Mixed-mode fatigue crack growth in FM73 bonded joints. Int J Adhes Adhes 2013;40:188–96
[25] Russell AJ, Street KN. Predicting interlaminar fatigue crack growth rates in compressively loaded laminates. Compos. Mater. Fatigue Fract., ASTM International; 1989, p. 162–78.
[26] Blanco N, Gamstedt EK, Asp LE, Costa J. Mixed-mode delamination growth in carbon-fibre composite laminates under cyclic loading. Int J Solids Struct 2004;41:4219–35.

A finite element study of fatigue crack propagation in single lap bonded joint with process-induced disbond

Liu, Yiding

2018-09-09

Yiding Liu, Stuart Lemanski, Xiang Zhang, et al., (2018) A finite element study of fatigue crack propagation in single lap bonded joint with process-induced disbond. International Journal of Adhesion and Adhesives, Volume 87, December 2018, pp. 164-172

https://doi.org/10.1016/j.ijadhadh.2018.10.005